RSC Advances

PAPER

View Article Online
View Journal | View Issue

Cite this: *RSC Adv.*, 2025, **15**, 28555

GCE surface coating with PdNiAg nanocatalysts to ensure high performance and stability in alcohol oxidation

Merve Akin,[ab] Muhammed Bekmezci,[ab] Cansu Catal,[ab] Guray Kaya[b] and Fatih Sen *[a]

Fuel cells as a clean energy source largely depend on the design of effective, long-lasting, and affordable electrocatalysts. In this context, chain-like palladium–nickel–silver (PdNiAg) nanoparticles (NPs) are synthesized using the chemical reduction method. The synthesized PdNiAg NPs are used for electro-oxidation of methanol, ethanol, and ethylene glycol. After oxidation studies, the anodic peak currents for methanol, ethylene glycol, and ethanol are found to be 43.92 mA cm^{-2}, 26.77 mA cm^{-2}, and 21.62 mA cm^{-2}, respectively. Long-term stability tests demonstrate that the catalyst exhibits a current density 1.6 times higher than that of ethylene glycol, and 2.15 times higher than that of ethanol in chronoamperometry (CA) analysis during methanol oxidation. The catalyst is shown to be a diffusion-controlled system for all three alcohols. It is observed to be tolerant to carbon monoxide (CO) and to have an electrochemically active surface area. The obtained catalyst exhibits high electrocatalytic performance, especially in methanol oxidation, and is a promising candidate for use in direct alcohol fuel cell (DAFC) systems. Within the scope of the study, catalysts with specific properties for different alcohol groups are synthesized, and important findings are presented to establish a position in the application field.

Received 20th April 2025
Accepted 21st July 2025

DOI: 10.1039/d5ra02762d

rsc.li/rsc-advances

1. Introduction

It is well documented that the advent of new technologies has resulted in a corresponding increase in energy consumption. The energy required is currently sourced from hydrocarbon-based fossil fuels. The utilization of fossil fuels, which are finite resources, has resulted in several adverse consequences, including global warming, environmental contamination, and a multitude of health issues. A variety of techniques have been employed to curb reliance on fossil fuels.[1] One of these methods, fuel cells, is a device that oxidizes fuels through a chemical reaction to generate electrical energy.[2] A fuel cell produces heat and water through a chemical reaction. While hydrogen plays a significant role in fuel cell operations, alcohol derivatives such as,[3] methanol,[4] ethanol,[5] 2-propanol,[6] formic acid[7] can also be used.

DAFCs exhibit several advantageous properties, such as ease of storage and transportation, high energy density, and low operating temperature.[8] DAFCs are capable of operating efficiently with low-molar-mass alcohols, making them suitable as power sources for a range of applications, including vehicle propulsion and portable electronic devices, at moderate temperatures.[9] Compared to gaseous hydrogen fuel, alcohols generally exhibit higher volumetric energy density and are easier to process, store, and transport.[10] DMFCs are attracting considerable attention due to the numerous advantages they offer, such as the absence of C–C bonds in methanol, higher power density, lower exhaust gas emissions, and ease of charging.[11] Despite offering significant advantages, commercialization of DMFCs is hampered by toxicity, slow kinetics of anodic methanol oxidation, and high cost.[12] Therefore, the potential of other alcohols, including glycerol, ethanol, methanol, and ethylene glycol, is also being investigated.[13] In this context, biofuel ethanol is considered the most promising option due to its superior energy density, non-toxicity, inherent renewability, and ease of use, management, and storage.[14] Methanol is the preferred alcohol for use in fuel cells due to its simple chemical structure, high energy density, and environmentally friendly nature.[15] Ethylene glycol, on the other hand, is attracting interest as a potential fuel cell component due to its favorable membrane permeability properties and increased fuel production capacity.[16]

The use of electrocatalysts with high electrocatalytic activity and stability is a key consideration for direct methanol fuel cell (DMFC) applications. In this context, catalyst selection is crucial for the catalytic performance of fuel cells, reducing efficiency losses in fuel cells, and improving energy density.[1,17,18] In catalyst synthesis, innovations in nanotechnology and materials science are enabling increased energy efficiency and fuel cell

[a]*Sen Research Group, Department of Biochemistry, Dumlupinar University, Kutahya, Türkiye. E-mail: fatihsen1980@gmail.com*
[b]*Department of Materials Science & Engineering, Faculty of Engineering, Dumlupinar University, Kutahya, Türkiye*

performance. It is generally accepted that the most commonly used anode materials in DMFCs is platinum (Pt) and Pt-based alloys.[19] However, various challenges such as the low toxicity tolerance of Pt, the presence of by-products, and the high cost of its commercialization seriously hinder the widespread adoption of this material.[20] At this point, research continues for more economical and stable catalysts that offer high catalytic activity, but do not contain Pt. Given the high cost of Pt-based catalysts, exploring cost-effective alternatives such as palladium (Pd) presents a promising option that could contribute to the wider adoption of fuel cell technology.[21] Furthermore, Pd has a strong ability to tolerate and remove adsorbed carbon monoxide (CO) formed during the electrooxidation of alcohols. This property is attributed to its ability to facilitate proton reduction and absorb and release hydrogen, enhancing its catalytic performance in alcohol oxidation reactions.[22] Bimetallic Pd alloys containing transition metals such as Pd–Ag, Pd–Ni, Pd–Cu, and Pd–Co exhibit improved catalytic activity compared to monometallic Pd and provide significant cost savings in fuel cell applications.[23,24] The lower cost and availability of Ag compared to Pd make it an ideal metal to produce bimetallic catalysts for fuel cells. Furthermore, the presence of Ag reduces the likelihood of CO-like substances poisoning by enhancing the adsorption properties.[25] In preventing CO poisoning, the Langmuir–Hinshelwood (L–H) mechanism is generally expressed by eqn (1) and (2). These reactions remove CO from the surface, and keep the catalyst active. CO poisoning is generally caused by the very strong adsorption of CO onto the catalyst surface. CO coats the active sites, stopping further reactions; in other words, the catalyst is "poisoned." The addition of metals such as Ag can alter the surface's adsorption capabilities, temporarily trapping CO on the surface and facilitating its removal. Studies on this topic indicate that the addition of Ag reduces CO poisoning.[26,27]

$$CO_{ads} + OH_{ads} \rightarrow COOH_{ads} \quad (1)$$

$$COOH_{ads} + OH_{ads} \rightarrow CO_2 + H_2O \quad (2)$$

Ni is the preferred catalyst due to its cost-effectiveness, ability to accelerate electron transfer, resistance to catalyst poisoning, and highly stable structure. PdNiAg NPs were synthesized in this study because of the superior advantages of Pd, Ni, and Ag. The high catalytic activity of Pd, the resistance of Ni to CO poisoning, and the oxygen adsorption ability of Ag combine to provide a higher reaction rate and yield. This combination enhances the adsorption of alcohol molecules on the surface by accelerating electron transfer, thereby potentially facilitating the provision of the requisite oxygen for the reaction in a more expedient manner.[28] Due to its cost-effectiveness and efficiency, this alloy provides long-lasting and stable energy production in alcohol-based fuel cells.

In this study, PdNiAg NPs were synthesized *via* a chemical reduction method and employed for the oxidation of methanol, ethanol, and ethylene glycol. The resulting NPs were also subjected to X-ray diffraction (XRD) and transmission electron microscopy (TEM) analysis. A catalyst for fuel cells was synthesized at a low cost. The study revealed that Pd-based catalysts offer a promising solution, as they can reduce costs and prevent deactivation of the active site by CO.

2. Material – method

2.1 Material

Palladium chloride ($PdCl_2$), nickel(II) acetate tetrahydrate ($Ni(OCOCH_3)_2 \cdot 4H_2O$), silver tetrachloride ($AgCl_4$), distilled water (dH_2O), sodium borohydride ($NaBH_4$), dimethylformamide (DMF), and Nafion D-521 were purchased from Sigma Aldrich.

2.2 Preparation of PdNiAg nanostructure using chemical reduction technique

First, synthesis studies were carried out. 10 mM $PdCl_2$, $Ni(OCOCH_3)_2 \cdot 4H_2O$, and AgCl were added to 20 mL dH_2O and stirred in argon gas for 1 hour. Then, the reducing agent sodium borohydride ($NaBH_4$) was added to the system and stirred in the Schlenk system until the gas leakage ended. The Schlenk system is a glassware system frequently used in chemical experiments conducted under inert atmospheric conditions. The system also utilizes a jacketed system to ensure temperature control. This system primarily ensures inertia in the environment. Water flow is ensured through the jacketed structure; this is important for controlling the reaction rate and preventing the formation of undesirable byproducts. This system ensures that the chemical reaction is completed in a safe, stable environment. At the end of sonication, the final mixture was centrifuged at 5000 rpm and washed 3 times with dH_2O. PdNiAg NP synthesis was achieved by drying in a 40 °C oven for 24 hours.

2.3 Electrochemical characterization

All electrochemical analyses were carried out with a potentiostat/galvanostatic (Gamry Reference 3000) device. Before electrochemical measurements, working electrodes were cleaned with alumina (Al_2O_3), ultrasonicated, and then washed with methanol. A three-electrode system was used for electrochemical measurements. This electrode system consists of a counter electrode (platinum plate), a working electrode (glassy carbon-GCE), and a reference electrode (Ag/AgCl). The resistance measurements of the working electrode were optimized by measuring with a multimeter. The optimized electrocatalyst coating was modified by drop-casting method. 10 mg NP powder, 500 μL dH_2O, 37.5 μL Nafion D-521, and 75 μL DMF were added to the modification solution and sonicated for 30 min. Then, a three-electrode system was established, and cycle voltammetry (CV), chronoamperometry (CA), long term (500 cycles), scan rate (SR), and electrochemical impedance spectroscopy (EIS) measurements were performed. The measurements were made in the potential range of −0.8 V to 0.2 V in 1 M KOH solutions containing methanol, ethanol, and ethylene glycol separately. To see the activity of the catalyst at different scan rates, SR measurements were performed in 1 M KOH solutions containing methanol, ethanol, and ethylene glycol separately at scan rates of 50 mV s^{-1}, 100 mV s^{-1}, 150 mV s^{-1}, 200 mV s^{-1}, and 250 mV s^{-1}. Methanol 2 M, ethanol 1 M,

and ethylene glycol 2 M were used in 500 cycle-graphs. At the same time, EIS measurements were performed. EIS measurements were performed in 1 M KOH solutions at a frequency range of 10 kHz–0.01 Hz.

2.4 Material structure

For the characterization of the obtained PdNiAg NPs, Transmission Electron Microscope (TEM (Hitachi – HT7800)), and X-ray diffraction (XRD) (Rigaku Miniflex) devices were used.

3. Results and discussion

3.1 XRD analysis

After the synthesis of PdNiAg NPs, crystal structure analysis was performed using XRD (Rigaku MiniFlex) as shown in Fig. 1. The XRD peaks at 38.1°, 44.4°, 64.6° and 77.5° at 2θ for to the standards (111), (200), (220), and (311) planes of face-centered cubic (FCC) Ag crystals, respectively, are shown. The orientation of Ag NPs is fixed in the (111) direction and also has a crystallographic plane with an FCC structure in the deposition process. The intense peak at $2\theta = 38.1°$ in the XRD pattern of Ag particles corresponds to the (111) plane of the surface-centered structure.[29] In the case of PdNiAg, the diffraction peaks observed in the Pd sample were well-defined and occurred at 40° (111), while the Ag sample exhibited diffraction peaks at 37.8° (200), 64.49° (220), and 77.46° (311). In the case of PdNi, the presence of diffraction peaks was observed at 45.56° (200), 67° (220) and 81.56° (311).[30] Furthermore, the small peak observed at 31.84° can be attributed to the oxidation of Ag. It shows that the Pd–Ni diffraction peak is located near the pure Pd diffraction peak, but with a small shift to its right. This is because Ni has a lower lattice constant than Pd, and Ni atoms partially displace the position of Pd in the crystals.[31] The findings are in accordance with those reported in the existing literature.[32,33]

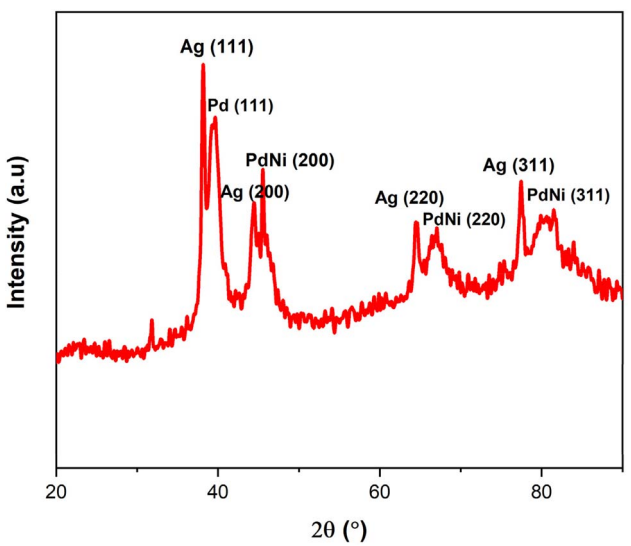

Fig. 1 XRD pattern of PdNiAg NPs.

3.2 TEM analysis

A transmission electron microscopy (TEM) analysis was conducted to examine the morphology of PdNiAg, and the results are presented in Fig. 2. In the transmission electron microscopy (TEM) image of PdNiAg, darker areas indicate the presence of high-atomic-number Pd and Ni, while lighter areas indicate the presence of Ag. Partial agglomeration observed in some areas can be attributed to the presence of impurities formed during material production.[34] Ag is widely distributed on the surface, indicating that Ag provides a suitable support material. Given the higher electron density of Pd and Ni NPs, it can be posited that their presence is more intense in darker regions. The particle size of the PdNiAg NPs was determined to be approximately 9.12 nm, with a standard error of 2.21 nm, based on the TEM images obtained in this context. In the calculations, the particle size was calculated by eliminating values that were found to be in excess of the standard. The findings are in close alignment with those documented in the existing literature.[35,36]

3.3 A study of the oxidation of different alcohols

Fig. 3 depicts the results of electro-oxidation studies conducted with a PdNiAg NP catalyst in a 1 M KOH solution for 1 M CH_3OH, 1 M C_2H_6O and 1 M $C_2H_6O_2$. Fig. 3a depicts the cyclic voltammetry (CV) curves for three distinct alcohols in the presence of the PdNiAg NP catalyst at a scan rate of 50 mV s^{-1}. The catalyst demonstrated high electrochemical performance for all three alcohols. Two distinct peaks were observed during both the forward and reverse scans, indicating characteristic oxidation behavior for each alcohol. As shown in Fig. 3b, the highest current density of 43.92 mA cm^{-2} was observed for CH_3OH, followed by $C_2H_6O_2$ oxidation with a current density of 26.77 mA cm^{-2}. In contrast, the lowest current density of 21.62 mA cm^{-2} was recorded in the oxidation of C_2H_6O. The results demonstrated that the catalyst exhibited the highest catalytic activity in methanol oxidation, which is believed to be due to its molecular structure and the nature of the carbon bonds involved. Activation of C–H bonds is the first step in the oxidation of methanol, and the cleavage of this bond is the primary determinant of catalytic activity. Oxidation of the C–OH group involves conversion to intermediate products such as formaldehyde and formic acid. This demonstrates the role of C–O bonds. At this point, the carbon bonds found in alcohols are important and can be said to influence activity. The capacity of the catalyst to oxidize adsorbed intermediate species, and its ability to withstand poisoning are purported to be related to the back peaks (I_b) in the CV analysis.[37,38] As seen in Table 1, an I_f/I_b ratio of 1.57 indicates that oxidation occurs to a large extent in the forward scan and that toxic intermediate species accumulate to a limited extent on the catalyst surface. This suggests that the catalyst has relatively high tolerance poisoning. In contrast, values close to or below 1.0, such as 0.9 and 0.67, indicate that toxic species like CO accumulate to a significant extent on the catalyst surface and that these species can only be oxidized in the reverse scan.[37–39] This suggests that the catalyst has lower poisoning tolerance, and that the active surfaces are temporarily blocked. These results indicate that the resulting catalyst

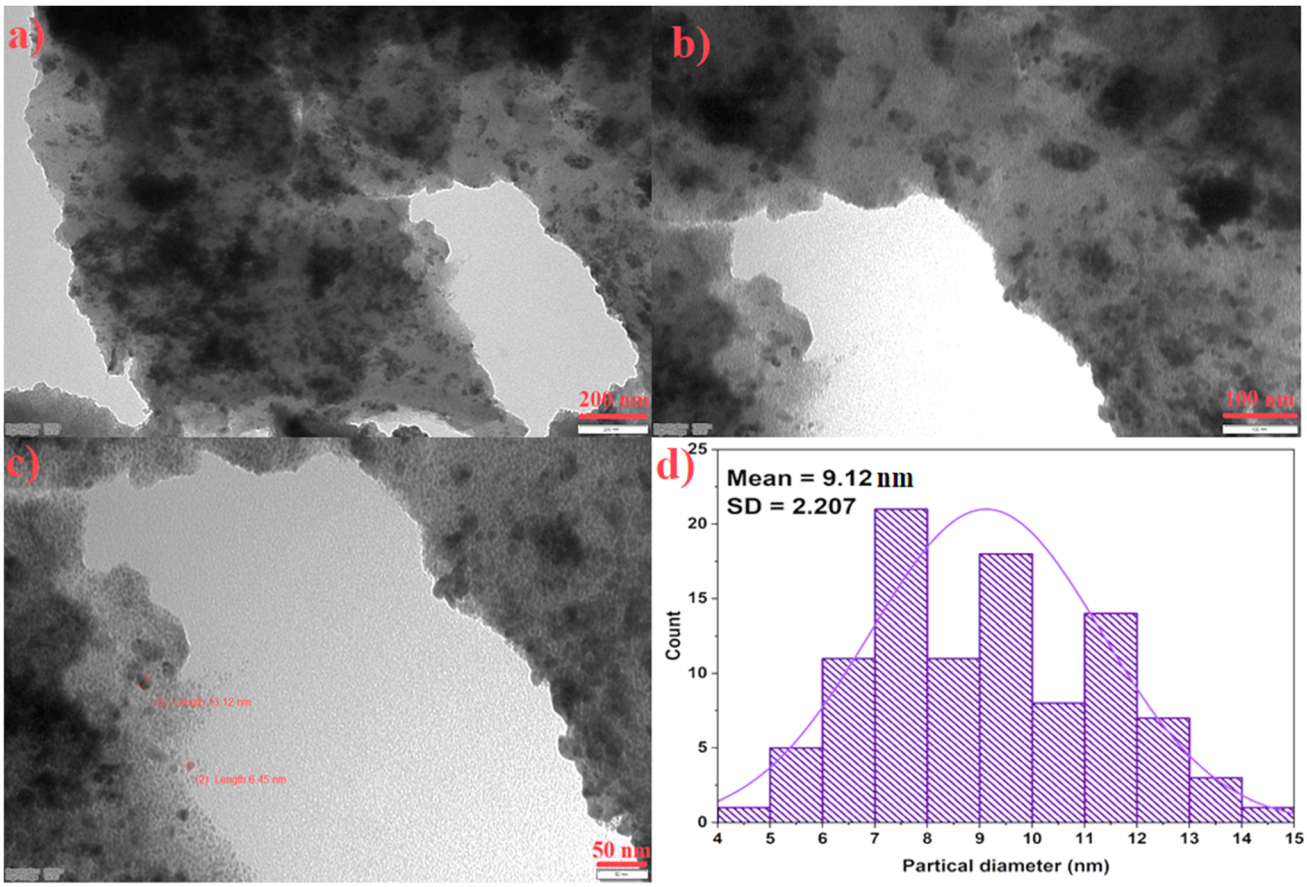

Fig. 2 TEM images of PdNiAg NPs (a) at 200 nm magnification, (b) at 100 nm magnification, (c) 50 nm magnification, (d) Histogram graph of PdNiAg NPs.

exhibits better CO tolerance in the case of ethylene glycol. Ethylene glycol is a larger and more complex molecule than methanol and ethanol; the toxic intermediates formed on the surface (*e.g.*, CO species) either bind more weakly to the catalyst or are more easily removed. This allows the catalyst to maintain activity by minimizing surface poisoning. In the oxidation of methanol and ethanol, species such as CO can bind tightly to the surface and poison the catalyst. Furthermore, because ethylene glycol adsorbs to the surface and has a different oxidation mechanism, the accumulation of toxic products is prevented. Because the oxidation potential and kinetics are more controlled, toxicity is reduced.

Fig. 4 shows the measurement results of 1 M methanol (Fig. 4a), 1 M ethanol (Fig. 4c), and 1 M ethylene glycol (Fig. 4e) oxidations at different scan rates and the R^2, slope values calculated accordingly (Fig. 4b, d and f). When the results are analyzed, it is seen that the current values increase as the scan rate increases for all alcohol types. This indicates that it can be controlled by mass transfer to regulate the electro-oxidation of alcohol on the produced catalyst.[40] It is observed that the peak flow points for anodic currents shift towards positive values. The reason for this change is thought to be due to the intermediate products resulting from oxidation studies. In CV analyses, the shift of the anodic peak current toward more positive potentials is generally attributed to the effects of toxic intermediates formed on the catalyst surface. Intermediates, particularly species containing aldehydes or carbonyl groups, can adsorb onto the catalyst surface and temporarily block active sites. This can slow down electron transfer at the surface, shifting the oxidation peak potential to more positive values. When examining the graphs in Fig. 4b, d and f, the linear relationship between peak currents and the square root of the scan rate initially indicates a diffusion-controlled process. However, the decrease in the slope of the curves as the scan rate increases indicates that the reactions are no longer controlled by diffusion, and are instead controlled by kinetics. This suggests that, especially at high scan rates, the system no longer depends on diffusion but on electron transfer kinetics at the surface.[40–42]

Within the scope of the study, CA and 500-cycle tests were performed for long stability tests. The CA test obtained at this point is as shown in Fig. 5a. In the results obtained as a result of 5000 s, the presence of current densities of 12.52 mA cm^{-2}, 7.48 mA cm^{-2}, 5.82 mA cm^{-2} in the presence of 1 M methanol, 1 M ethylene glycol, and 1 M ethanol, respectively. This showed that oxidation was continuing at the end of 5000 s, and the catalyst exhibited a stable behavior. The results of 500 cycles of the obtained catalyst for different alcohols are as shown in Fig. 5b–

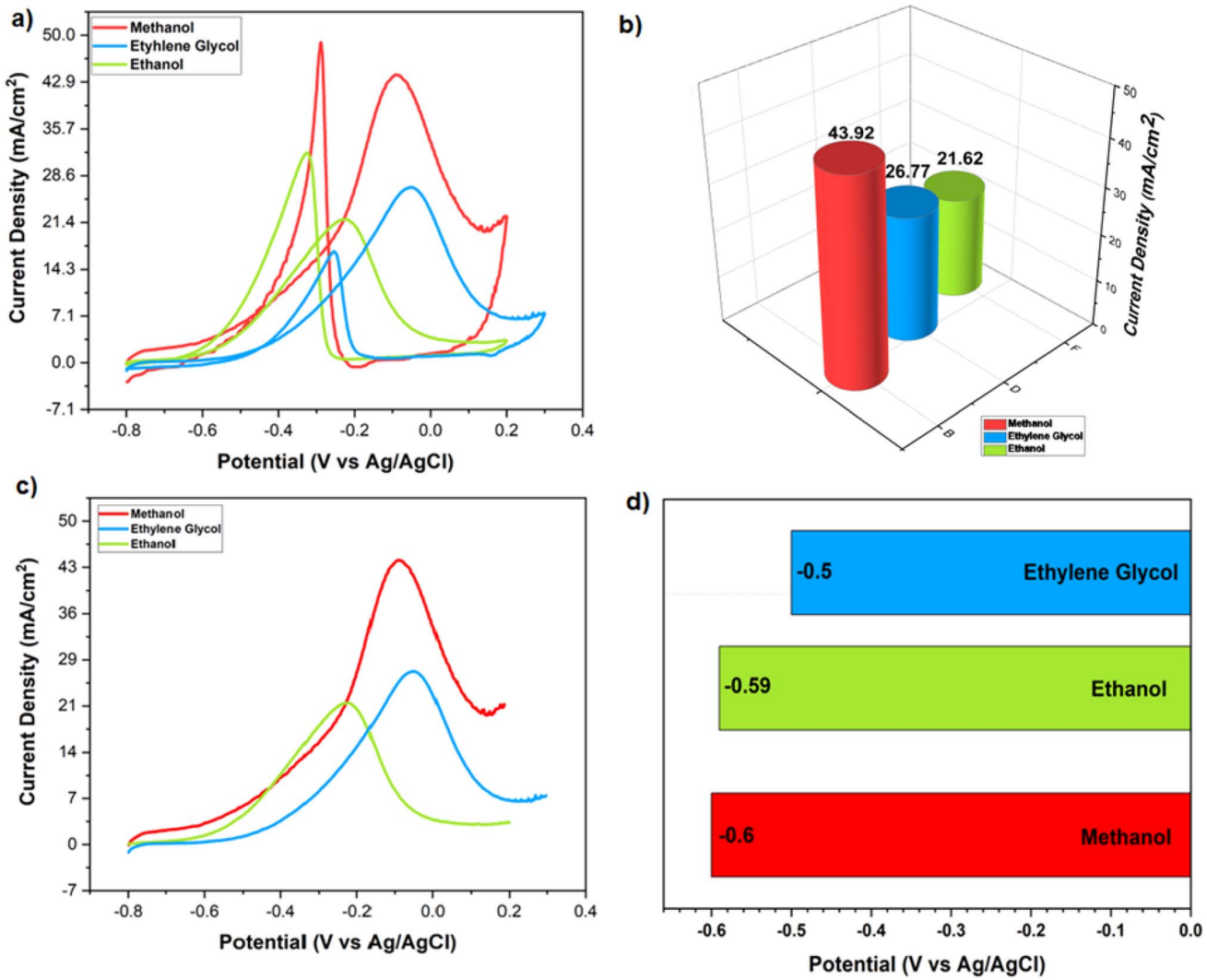

Fig. 3 Electrochemical measurements in 1 M methanol, 1 M ethanol and 1 M ethylene glycol for PdNiAg NPs, (a) comparison of CV curves of three different alcohol oxidations for PdNiAg, (b) peak current values obtained from CV results, (c) LSV curves of three different alcohol oxidations for PdNiAg, (d) comparison of the initial potentials obtained from the LSV graph.

Table 1 I_f, I_b and I_f/I_b ratios for PdNiAg

Alcohol	I_f (mA cm^{-2})	I_b (mA cm^{-2})	I_f/I_b (mA cm^{-2})
CH_3OH	43.92	48.75	0.9
$C_2H_6O_2$	26.77	17	1.57
C_2H_6O	21.62	32	0.67

d. In the presence of 2 M methanol and 2 M ethylene glycol, a high increase in current density was observed until the 75th cycle, and then a decrease in current density was observed. In the presence of 1 M ethanol, it was observed that at the end of 500 cycles, a slight but continuous increase in peak current density was achieved, and close current values were observed. A high increase in methanol can be attributed to the fact that it has a low carbon chain and leaves fewer by-products on the surface. The decrease after a while can be attributed to the formation of intermediates such as formic acid and the blocking of active sites by toxic substances such as CO. In the case of ethylene glycol, the two-carbon content may pose a challenge for oxidation. The slight increase in current in the results shows that the catalyst shows a very good interaction with ethylene glycol. Although ethanol has a more complex oxidation mechanism than methanol, the catalyst showed a very stable behavior. It can be said that the fact that it is very difficult to break carbon–carbon bonds in ethanol provides a more constant current density without overloading the catalyst. In Fig. 5e, the EIS measurement result is shown. The charge transfer resistance is related to the semicircular diameter of the Nyquist plot constructed using EIS measurements.[43] The fact that the EIS graph is partially wide can be seen that intermediate products can accumulate on the surface and make load transfer difficult.

The relatively high catalytic performance of PdNiAg NPs in methanol oxidation is based on the synergistic effects provided by the alloy structure, surface properties, and structural

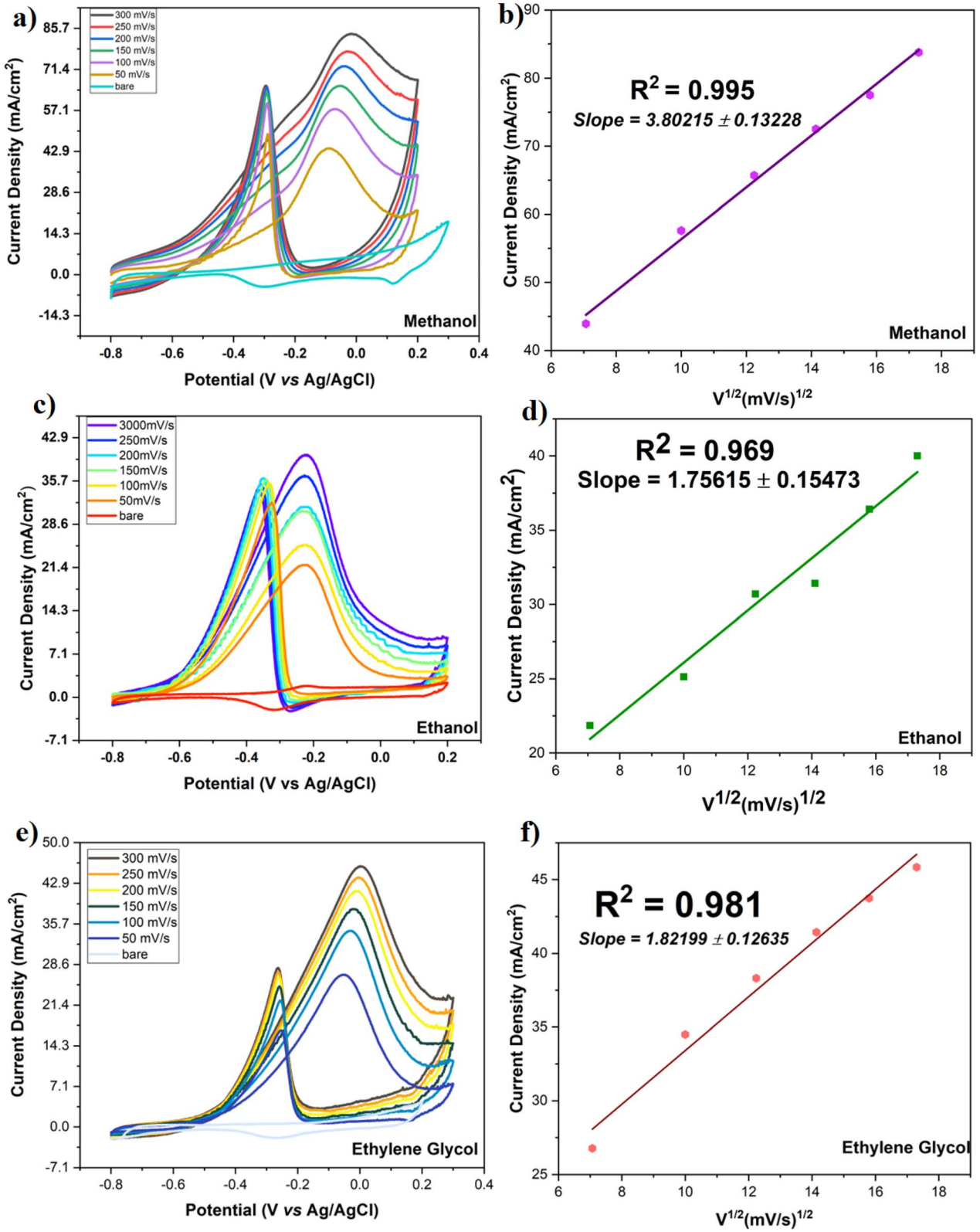

Fig. 4 (a) Scan rate plot for PdNiAg in 1 M methanol, and in 1 M KOH solution, (b) current density plot *versus* square root of the scan rate in 1 M methanol oxidation, (c) scan rate plot for PdNiAg in 1 M ethanol and 1 M KOH solution, (d) current density plot *versus* square root of the scan rate in 1 M ethanol oxidation, (e) scan rate plot for PdNiAg in 1 M ethylene glycol, and 1 M KOH solution, (f) current density plot *versus* square root of the scan rate in 1 M ethylene glycol oxidation.

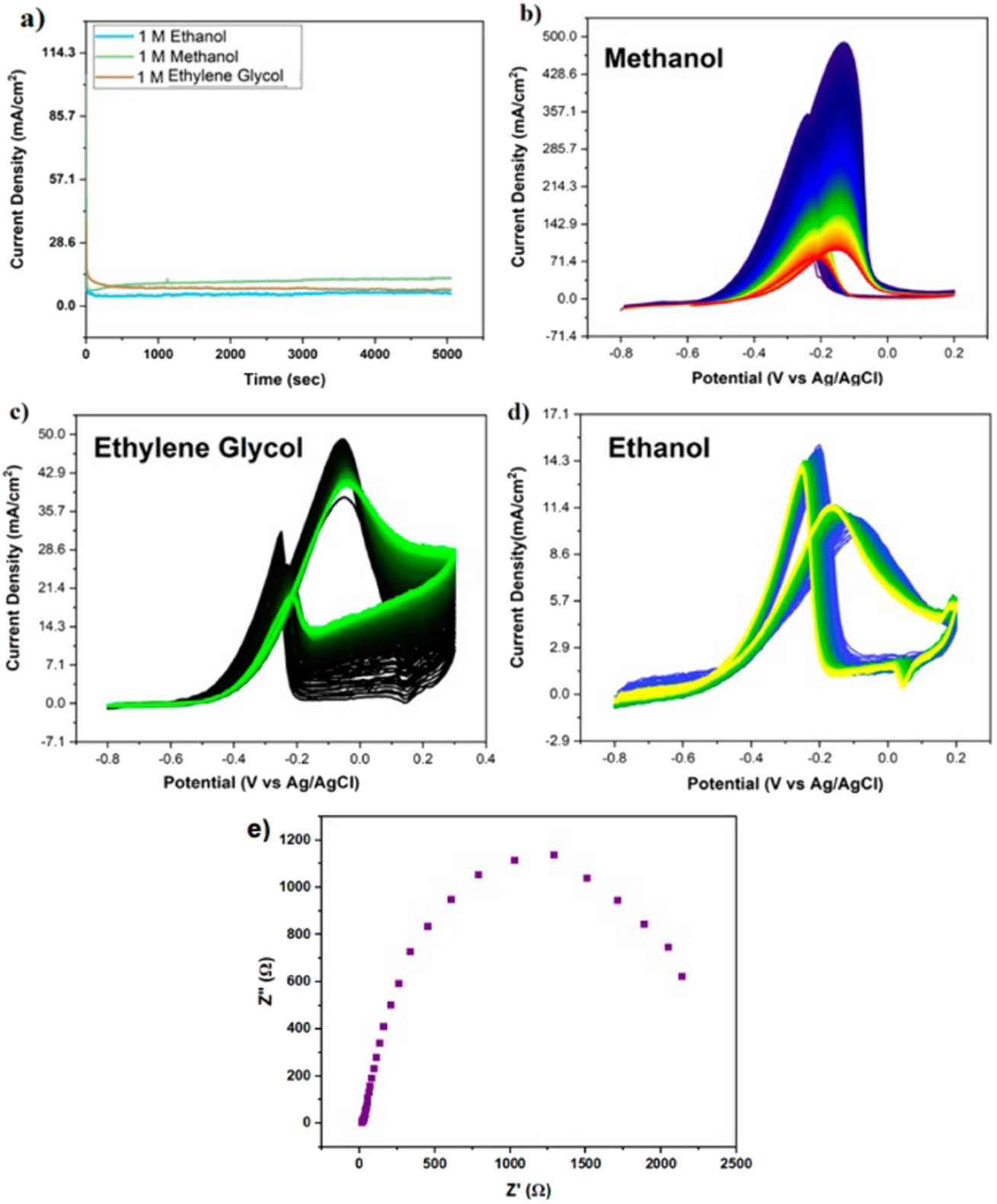

Fig. 5 (a) CA plot obtained in 1 M methanol, 1 M ethanol and 1 M ethylene glycol for PdNiAg NPs, (b) long term stability for PdNiAg in 2 M methanol, and 1 M KOH solution for 500 cycles , (c) long term stability for PdNiAg in 2 M ethylene glycol, and 1 M KOH solution for 500 cycles, (d) long term stability for PdNiAg in 1 M ethanol, and in 1 M KOH solution for 500 cycles, (e) Nyquist plot for PdNiAg.

Table 2 Comparison of the results obtained in current study and the literature studies

Electrocatalysis	Solution	Alcohol	Scan rate (mV s^{-1})	Anodic peak current (mA cm^{-2})	References
Pd/CNT	1 M KOH	1 M CH_3OH	20 mV s^{-1}	24.9	44
$MnCo_2O_4/NiCo_2O_4$/rGO	2 M KOH	0.5 M CH_3OH	20 mV s^{-1}	24.76 mA cm^{-2}	45
PdAg-ANTs/GC	1 M KOH	1 M C_2H_6O	50 mV s^{-1}	13.58 mA cm^{-2}	46
PdAg-NS/GC	1 M KOH	1 M C_2H_6O	50 mV s^{-1}	2.34 mA cm^{-2}	47
PdNiAg@rGO/$CoMoO_4$	1 M KOH	1 M $C_2H_6O_2$	50 mV s^{-1}	196.58 mA cm^{-2}	48
Au-decorated PdRu nanopopcorns	1 M KOH	1 M $C_2H_6O_2$	50 mV s^{-1}	22.1 mA cm^2	49
PtCu	1 M KOH	1 M CH_3OH	50 mV s^{-1}	187.7 mA cm^{-2}	
PdNiAg	1 M KOH	1 M CH_3OH	50 mV s^{-1}	43.92 mA cm^{-2}	This work
PdNiAg	1 M KOH	1 M $C_2H_6O_2$	50 mV s^{-1}	26.77 mA cm^{-2}	This work
PdNiAg	1 M KOH	1 M C_2H_6O	50 mV s^{-1}	21.62 mA cm^{-2}	This work

stability. While Pd serves as the active center in methanol oxidation, Ni contributes to the easier removal of reaction intermediates (especially CO) from the surface by modifying the electronic structure of Pd, thus increasing the catalyst's resistance to CO poisoning. While Ag is not directly active, it increases the surface area by allowing Pd to be distributed more homogeneously and contributes to the stability of the NPs. The small and homogeneously distributed NPs, approximately 9 nm in size, observed in TEM images, offer more active sites due to their high surface area, which directly increases catalytic activity. Furthermore, the structural stability of the PdNiAg alloy provides a significant advantage for long-term and efficient catalysis. For these reasons, PdNiAg NPs exhibit high performance in electrochemical applications such as alcohol oxidation.

Table 2 provides a comparison of alcohol oxidation studies with various electrocatalysts to compare the results obtained with the literature. According to the literature studies, it is seen that the addition of NiAg to Pd increases electrocatalytic activity considerably. It is also observed that the presence of Ni in the catalyst provides high electrocatalytic activity, especially in ethanol and ethylene glycol oxidation. The results agree with the literature, and it can be said that the obtained catalyst is promising in alcohol fuel cell studies.

4. Conclusion

In this study, PdNiAg NPs were synthesized by the chemical reduction method for alcohol oxidation investigations. The crystal structure formation of PdNiAg was revealed by XRD analysis, and the particle size of PdNiAg obtained by TEM results was found to be 9.12 nm. For the electrooxidation of methanol, ethanol and ethylene glycol, the characterized PdNiAg NPs were used in an alkaline medium. In the studies on alcohol oxidation, current densities of 43.92 mA cm^{-2}, 26.77 mA cm^{-2}, and 21.62 mA cm^{-2} were obtained for methanol, ethylene glycol, and ethanol respectively. The results showed that the obtained catalyst provided one of the highest electrocatalytic activity for methanol oxidation. In the I_f/I_b values obtained for different alcohol oxidation, it was concluded that the intermediate product tolerance was higher for methanol and ethylene glycol. From the scan rate graphs obtained, it was observed that the systems were diffusion-controlled, and the LSV results showed that the catalyst started at an earlier potential in methanol oxidation. In CA and 500-cycle long-term stability tests, it is seen that the catalyst in the presence of methanol shows 1.6 times more current density at the end of 5000 s and provides an increase in current density over 500 cycles. In the presence of ethylene glycol and ethanol, it can be said that the catalysts gave a very good result in the long-term stability test. The results are very promising in the oxidation of alcohols such as ethanol, methanol, and ethylene glycol, with the PdNiAg electrocatalyst showing very high electrocatalytic activity and high stability. Due to its excellent performance, economic benefits, and stability, this electrocatalyst can be used in studies on alcohol oxidation.

Conflicts of interest

There are no conflicts to declare.

Data availability

Data from this study will be made available upon request.

References

1 R. Bayat, A. El Attar, M. Akin, M. Bekmezci, M. El Rhazi and F. Sen, Copper nanoparticle modified chain-like platinum nanocomposites for electro-oxidation of C1-, C2-, and C3-type alcohols, *Int. J. Hydrogen Energy*, 2024, **51**, 1577–1586, DOI: 10.1016/J.IJHYDENE.2023.09.255.
2 J. M. DeCicco, Fuel cell vehicles, *Encycl. Energy*, 2004, 759–770, DOI: 10.1016/B0-12-176480-X/00181-9.
3 I. Dincer and H. Ishaq, Hydrogen production methods, *Renewable Hydrogen Prod.*, 2022, 35–90, DOI: 10.1016/B978-0-323-85176-3.00005-6.
4 X. Zhang, L. Hui, D. Ya, J. Li, X. Chen, H. Wu and Y. Li, Defect Rich Structure Activated 3D Palladium Catalyst for Methanol Oxidation Reaction, *Angew. Chem., Int. Ed.*, 2023, **62**(40), 1–8, DOI: 10.1002/anie.202308968.
5 Y. Casas, J. Dewulf, L. E. Arteaga-Pérez, M. Morales, H. Van Langenhove and E. Rosa, Integration of solid oxide fuel cell in a sugar–ethanol factory: analysis of the efficiency and the environmental profile of the products, *J. Clean*

Prod., 2011, **19**, 1395–1404, DOI: 10.1016/J.JCLEPRO.2011.04.018.

6 M. Brodt, K. Müller, J. Kerres, I. Katsounaros, K. Mayrhofer, P. Preuster, P. Wasserscheid and S. Thiele, The 2-propanol fuel cell: a review from the perspective of a hydrogen energy economy, *Energy Technol.*, 2021, **9**, 2100164, DOI: 10.1002/ENTE.202100164.

7 H. Cheng, J. Wang, C. Wu and Z. Liu, Electrocatalysts for formic acid-powered PEM fuel cells: challenges and prospects, *Energy Mater. Adv.*, 2023, **4**, DOI: 10.34133/ENERGYMATADV.0067.

8 K. Elsaid, S. Abdelfatah, A. M. Abdel Elabsir, R. J. Hassiba, Z. K. Ghouri and L. Vechot, Direct alcohol fuel cells: assessment of the fuel's safety and health aspects, *Int. J. Hydrogen Energy*, 2021, **46**, 30658–30668, DOI: 10.1016/J.IJHYDENE.2020.12.009.

9 E. Antolini and E. R. Gonzalez, Alkaline direct alcohol fuel cells, *J. Power Sources*, 2010, **195**, 3431–3450, DOI: 10.1016/J.JPOWSOUR.2009.11.145.

10 M. Yue, H. Lambert, E. Pahon, R. Roche, S. Jemei and D. Hissel, Hydrogen energy systems: a critical review of technologies, applications, trends and challenges, *Renewable Sustainable Energy Rev.*, 2021, **146**, 111180, DOI: 10.1016/J.RSER.2021.111180.

11 G. Gwak, K. Lee, S. Ferekh, S. Lee and H. Ju, Analyzing the effects of fluctuating methanol feed concentration in active-type direct methanol fuel cell (DMFC) systems, *Int. J. Hydrogen Energy*, 2015, **40**, 5396–5407, DOI: 10.1016/J.IJHYDENE.2015.01.062.

12 H. Burhan, K. Arikan, M. H. Alma, M. S. Nas, H. Karimi-Maleh, F. Şen, F. Karimi and Y. Vasseghian, Highly efficient carbon hybrid supported catalysts using nano-architecture as anode catalysts for direct methanol fuel cells, *Int. J. Hydrogen Energy*, 2023, **48**, 6657–6665, DOI: 10.1016/J.IJHYDENE.2021.12.141.

13 R. Bayat, M. Akin, M. Bekmezci, G. Gules, I. Isik and F. Sen, Facile synthesis of fiber-reinforced catalyst for high performance ethanol and 2-propanol oxidation, *Energy Technol.*, 2024, **12**, 2301063, DOI: 10.1002/ENTE.202301063.

14 S. R. Chowdhury, K. Kanti Bera, A. Ray, P. Bera, T. Maiyalagan and S. K. Bhattacharya, Synergistic catalytic activity of palladium–silver alloy nanoparticle for anodic oxidation of ethanol in alkali, *Int. J. Hydrogen Energy*, 2021, **46**, 14212–14224, DOI: 10.1016/J.IJHYDENE.2020.11.113.

15 B. Baruah and P. Deb, Performance and application of carbon-based electrocatalysts in direct methanol fuel cell, *Mater. Adv.*, 2021, **2**, 5344–5364, DOI: 10.1039/D1MA00503K.

16 Z. Pan, Y. Bi and L. An, Performance characteristics of a passive direct ethylene glycol fuel cell with hydrogen peroxide as oxidant, *Appl. Energy*, 2019, **250**, 846–854, DOI: 10.1016/J.APENERGY.2019.05.072.

17 F. Karimi, M. Akin, R. Bayat, M. Bekmezci, R. Darabi, E. Aghapour and F. Sen, Application of quasihexagonal Pt@PdS2-MWCNT catalyst with high electrochemical performance for electro-oxidation of methanol, 2-propanol, and glycerol alcohols for fuel cells, *Mol. Catal.*, 2023, **536**, 112874, DOI: 10.1016/J.MCAT.2022.112874.

18 M. Akin, M. Bekmezci, R. Bayat, I. Isik and F. Sen, Ultralight covalent organic frame graphene aerogels modified platinum–magnetite nanostructure for direct methanol fuel cell, *Fuel*, 2024, **357**, 129771, DOI: 10.1016/J.FUEL.2023.129771.

19 Z. A. Che Ramli, J. Pasupuleti, T. S. Tengku Saharuddin, Y. N. Yusoff, W. N. R. W. Isahak, L. Baharudin, C. Tak Yaw, S. P. Koh and S. Tiong Kiong, Electrocatalytic activities of platinum and palladium catalysts for enhancement of direct formic acid fuel cells: an updated progress, *Alexandria Eng. J.*, 2023, **76**, 701–733, DOI: 10.1016/J.AEJ.2023.06.069.

20 J. Ren, J. Zhang, C. Yang, Y. Yang, Y. Zhang, F. Yang, R. Ma, L. Yang, H. He and H. Huang, Pd nanocrystals anchored on 3D hybrid architectures constructed from nitrogen-doped graphene and low-defect carbon nanotube as high-performance multifunctional electrocatalysts for formic acid and methanol oxidation, *Mater Today Energy*, 2020, **16**, 100409, DOI: 10.1016/J.MTENER.2020.100409.

21 J. D. Sinniah, W. Y. Wong, K. S. Loh, R. M. Yunus and S. N. Timmiati, Perspectives on carbon-alternative materials as Pt catalyst supports for a durable oxygen reduction reaction in proton exchange membrane fuel cells, *J. Power Sources*, 2022, **534**, 231422, DOI: 10.1016/J.JPOWSOUR.2022.231422.

22 M. Mansor, S. N. Timmiati, A. M. Zainoodin, K. M. Pa'ad and K. L. Lim, Investigation of palladium-mesostructured silica nanoparticles (Pd-MSN) as anode electrocatalyst for alkaline direct methanol fuel cell, *Chem. Phys. Lett.*, 2021, **785**, 139125, DOI: 10.1016/J.CPLETT.2021.139125.

23 S. R. Chowdhury, P. Mukherjee and S. kumar Bhattachrya, Palladium and palladium–copper alloy nano particles as superior catalyst for electrochemical oxidation of methanol for fuel cell applications, *Int. J. Hydrogen Energy*, 2016, **41**, 17072–17083, DOI: 10.1016/J.IJHYDENE.2016.05.239.

24 M. A. Ud Din, M. Idrees, S. Jamil, S. Irfan, G. Nazir, M. A. Mudassir, M. S. Saleem, S. Batool, N. Cheng and R. Saidur, Advances and challenges of methanol-tolerant oxygen reduction reaction electrocatalysts for the direct methanol fuel cell, *J. Energy Chem.*, 2023, **77**, 499–513, DOI: 10.1016/J.JECHEM.2022.11.023.

25 Y. Zhao, X. Zhang and Z. Yang, Efficient capturing and oxidation of CO through bimetallic surface alloying on WC (0001), *J. Alloys Compd.*, 2020, **844**, 156125, DOI: 10.1016/J.JALLCOM.2020.156125.

26 K. Sawabe and A. Satsuma, Theoretical study on carbon monoxide adsorption on unsupported and γ-Al_2O_3-supported silver nanoparticles: size, shape, and support effects, *ACS Omega*, 2022, **7**, 4405–4412, DOI: 10.1021/ACSOMEGA.1C06208.

27 Z. Zhuang, G. Wang, W. Zhao, R. Yang, Y. Zhou and W. Zhu, Silver-doped porous copper catalysts for efficient resource utilization of CO-containing flue gases, *ACS Environ. Au*, 2025, **5**, 287–297, DOI: 10.1021/ACSENVIRONAU.4C00121.

28 R. M. Al Soubaihi, K. M. Saoud, A. Awadallah-F, A. M. Elkhatat, S. A. Al-Muhtaseb and J. Dutta, Investigation of palladium catalysts in mesoporous silica

support for CO oxidation and CO_2 adsorption, *Heliyon*, 2023, **9**, e18354, DOI: 10.1016/J.HELIYON.2023.E18354.

29 *Nano Silver-Coated Polypropylene Water Filter: I. Manufacture by Electron Beam Gun Using a Modified Balzers 760 Machine*, n.d., https://www.researchgate.net/publication/234840473_Nano_silver-coated_polypropylene_water_filter_I_Manufacture_by_electron_beam_gun_using_a_modified_balzers_760_machine?_tp=eyJjb250ZXh0Ijp7ImZpcnN0UGFnZSI6Il9kaXJlY3QiLCJwYWdlIjoiX2RpcmVjdCJ9fQ, accessed 25 March, 2024.

30 M. Yurderi, A. Bulut, M. Zahmakiran and M. Kaya, Carbon supported trimetallic PdNiAg nanoparticles as highly active, selective and reusable catalyst in the formic acid decomposition, *Appl. Catal., B*, 2014, **160–161**, 514–524, DOI: 10.1016/J.APCATB.2014.06.004.

31 G. Wang, D. Li, Y. Zuo, Y. Tang, X. Zhang and X. Zhao, The improvement of hardness and corrosion resistance of electroplated Pd-Ni film on 316L stainless steel by $CeCl_3$, *Coatings*, 2020, **10**, 161, DOI: 10.3390/COATINGS10020161.

32 M. S. Khan, R. Khattak, A. Khan, Q. Chen, J. Nisar, Z. Iqbal, A. Rashid, A. W. Kamran, I. Zekker, M. Zahoor, K. J. Alzahrani and G. E. S. Batiha, Synthesis and characterizations of PdNi carbon supported nanomaterials: studies of electrocatalytic activity for oxygen reduction in alkaline medium, *Molecules*, 2021, **26**(11), 3440, DOI: 10.3390/MOLECULES26113440.

33 X. Zhao, X. Zhu, K. Wang, J. Lv, S. Chen, G. Yao, J. Lang, F. Lv, Y. Pu, R. Yang, B. Zhang, Z. Jiang and Y. Wan, Palladium catalyzed radical relay for the oxidative cross-coupling of quinolines, *Nat. Commun.*, 2022, **13**, 4180, DOI: 10.1038/S41467-022-31967-0.

34 M. Malatesta, Transmission electron microscopy as a powerful tool to investigate the interaction of nanoparticles with subcellular structures, *Int. J. Mol. Sci.*, 2021, **22**, 22, DOI: 10.3390/IJMS222312789.

35 I. Feliciano-Ramos, E. O. Ortiz-Quiles, L. Cunci, D. C. Díaz-Cartagena, O. Resto and C. R. Cabrera, Unsupported palladium nanoparticles for ethanol cyclic voltammetric sensing in alkaline media, *J. Solid State Electrochem.*, 2016, **20**, 1011–1017, DOI: 10.1007/S10008-015-3046-X.

36 J. Zheng, S. Zhou, S. Gu, B. Xu and Y. Yan, Size-dependent hydrogen oxidation and evolution activities on supported palladium nanoparticles in acid and base, *J. Electrochem. Soc.*, 2016, **163**, F499–F506, DOI: 10.1149/2.0661606JES.

37 F. Karimi, M. Akin, R. Bayat, M. Bekmezci, R. Darabi, E. Aghapour and F. Sen, Application of quasihexagonal Pt@PdS2-MWCNT catalyst with high electrochemical performance for electro-oxidation of methanol, 2-propanol, and glycerol alcohols for fuel cells, *Mol. Catal.*, 2023, **536**, 112874, DOI: 10.1016/J.MCAT.2022.112874.

38 R. Bayat, A. El Attar, M. Akin, M. Bekmezci, M. El Rhazi and F. Sen, Copper nanoparticle modified chain-like platinum nanocomposites for electro-oxidation of C1-, C2-, and C3-type alcohols, *Int. J. Hydrogen Energy*, 2024, **51**, 1577–1586, DOI: 10.1016/J.IJHYDENE.2023.09.255.

39 X. Qi, N. Ye, R. Zhang, Z. Jiang and T. Fang, Boosting the activity and CO tolerance for methanol oxidation reaction in alkaline media by constructing the Pt-TMNs electrocatalysts, *Fuel*, 2023, **350**, 128773, DOI: 10.1016/J.FUEL.2023.128773.

40 F. Karimi, M. Akin, R. Bayat, M. Bekmezci, R. Darabi, E. Aghapour and F. Sen, Application of quasihexagonal Pt@PdS2-MWCNT catalyst with high electrochemical performance for electro-oxidation of methanol, 2-propanol, and glycerol alcohols for fuel cells, *Mol. Catal.*, 2023, **536**, 112874, DOI: 10.1016/J.MCAT.2022.112874.

41 H. Javan, E. Asghari, H. Ashassi-Sorkhabi and M. Moradi-Haghighi, Nickel nanoparticles decorated on carbon quantum dots as a novel non-platinum catalyst for methanol oxidation; a green, low-cost, electrochemically-synthesized electrocatalyst, *Chem. Eng. Sci.*, 2020, **217**, 115534, DOI: 10.1016/J.CES.2020.115534.

42 R. Bayat, A. El Attar, M. Akin, M. Bekmezci, M. El Rhazi and F. Sen, Copper nanoparticle modified chain-like platinum nanocomposites for electro-oxidation of C1-, C2-, and C3-type alcohols, *Int. J. Hydrogen Energy*, 2024, **51**, 1577–1586, DOI: 10.1016/J.IJHYDENE.2023.09.255.

43 M. Akin, M. Bekmezci, R. Bayat, I. Isik and F. Sen, Ultralight covalent organic frame graphene aerogels modified platinum-magnetite nanostructure for direct methanol fuel cell, *Fuel*, 2024, **357**, 129771, DOI: 10.1016/J.FUEL.2023.129771.

44 W. Chen, Y. Zhang and Z. Zhu, Effects of cerium oxides on the catalytic performance of Pd/CNT for methanol oxidation, *Chem. Res. Chin. Univ.*, 2019, **35**, 133–138, DOI: 10.1007/S40242-019-8097-5/METRICS.

45 M. B. Askari, S. Azizi, M. T. T. Moghadam, M. Seifi, S. M. Rozati and A. Di Bartolomeo, $MnCo_2O_4$/$NiCo_2O_4$/rGO as a catalyst based on binary transition metal oxide for the methanol oxidation reaction, *Nanomaterials*, 2022, **12**, 4072, DOI: 10.3390/NANO12224072.

46 C. Peng, W. Yang, E. Wu, Y. Ma, Y. Zheng, Y. Nie, H. Zhang and J. Xu, PdAg alloy nanotubes with porous walls for enhanced electrocatalytic activity towards ethanol electrooxidation in alkaline media, *J. Alloys Compd.*, 2016, DOI: 10.1016/j.jallcom.2016.12.198.

47 C. Peng, Y. Hu, M. Liu and Y. Zheng, Hollow raspberry-like PdAg alloy nanospheres: high electrocatalytic activity for ethanol oxidation in alkaline media, *J. Power Sources*, 2015, **278**, 69–75, DOI: 10.1016/J.JPOWSOUR.2014.12.056.

48 Z. Wan, X. Bai, H. Mo, J. Yang, Z. Wang and L. Zhou, Multi-porous NiAg-doped Pd alloy nanoparticles immobilized on reduced graphene oxide/$CoMoO_4$ composites as a highly active electrocatalyst for direct alcohol fuel cell, *Colloids Surf., A*, 2021, **614**, 126048, DOI: 10.1016/J.COLSURFA.2020.126048.

49 H. Xu, P. Song, B. Yan, J. Wang, F. Gao, Y. Zhang and Y. Du, Superior ethylene glycol electrocatalysis enabled by Au-decorated PdRu nanopopcorns, *J. Electroanal. Chem.*, 2018, **814**, 31–37, DOI: 10.1016/J.JELECHEM.2018.02.034.